A THERMODYNAMIC AND EXPERIMENTAL STUDY OF LOW-ALLOY STEELS AFTER CARBONITRIDING IN A LOW-PRESSURE ATMOSPHERE

T. Marray,[1, 2] **P. Jacquet,**[1, 3] **M. Mansori,**[4] **A. Fabre,**[2] **and L. Barrallier**[2]

The effect of the composition of two steels (*B* and 6MnCr5) on precipitation of undesirable phases (carbides, nitrides and carbonitrides) under thermochemical treatment (low-pressure or vacuum carbonitriding) is investigated. Metallographic and x-ray diffraction studies and thermodynamic computations are performed.

Key words: carbonitriding in low-pressure atmospheres, vacuum carbonitriding, carbides, carbonitrides, alloy steel.

INTRODUCTION

In many practical cases the performance of a structural component depends on the mechanical properties of the surface [1]. Many methods of thermochemical treatment are used to raise the properties of the surface, such as gas carburizing [2 – 4], carbonitriding [2, 4], and low-pressure carburizing (vacuum carburizing) [5 – 7].

Conventional methods of thermochemical treatment of steel are based on diffusion of carbon and (or) nitrogen in surface layers. Carbonitriding, which is known to be more advantageous than standard carburizing, especially at a low thickness of the hardened layer, is commonly performed in conventional atmospheres [4, 8]. Published information on low-pressure carbonitriding (LPCN) is quite scarce [9, 10].

Due to the intrinsic nonequilibrium of the low-pressure treatment the conventional methods [11, 12] are inapplicable for controlling such processes. For this reason, we used computer simulation to predict the relation between the effective thickness of the hardened layer and the accurate profiles of the distribution of carbon and nitrogen in steels [13 – 18].

On the whole, the process of carbonitriding (developed on the basis of carburizing) is performed in two stages. The first stage, which is usually termed a boost one, provides delivery of a high content of carbon and nitrogen from the atmosphere to the surface. The second stage, i.e., diffusion, consists in keeping the parts at a constant temperature in vacuum (after cutting off the gas flow to the atmosphere).

Such division of the process of LPCN makes it possible to avoid transition through the maximum solubility of carbon in the austenite and hence to prevent precipitation of undesirable phases such as $M_{23}C$ and M_7C_3 carbides and M(C, N) carbonitrides. Earlier studies of alloys of the Fe – Cr – C system treated in a conventional manner have revealed formation of microstructures represented by α-ferrite and M_3C, M_7C_3 and $M_{23}C_6$ complex carbides depending on the alloying of the metal [19, 20].

The aim of the present work was an experimental and computational study of the effect of the composition of steels on undesirable precipitation in the process of low-pressure carbonitriding.

METHODS OF STUDY

Studied Steels

The samples for carbonitriding were fabricated from two low-alloy steels the chemical compositions of which are given in Table 1. The low content of carbon in the steels guarantees a tough core in the parts after carbonitriding.

All the samples had a cylindrical shape and were $\varnothing 16 \times 20$ mm in size. Both end faces were ground before the treatment.

Low-Pressure Carbonitriding

Most of the results presented were obtained using a commercial BMI Fours Industriels furnace that had earlier been

---

[1] Laboratoire de Science des Matériaux, ECAM, Lyon, France.
[2] Arts et Métiers ParisTech, MSMP, Aix en Provence, France.
[3] Arts et Métiers ParisTech, LaBoMaP, Cluny, France.
[4] Laboratoire de Chimie des Matériaux et Evironnement, Université Cadi Ayyad, Marrakech, Maroc.

TABLE 1. Nominal Chemical Compositions of the Steels of Grades B and 16MnCr5

| Steel	Content of elements, wt.%							
	C	Cr	Mn	V	W	Mo	Ni	Si
B	0.18	3.12	0.34	0.7	0.45	0.46	0.4	0.19
16MnCr5	0.16	1.00	1.00	–	–	–	–	0.40

used for developing a sensor for monitoring processes of low-pressure carburizing [6]. The samples were subjected to LPCN at 860°C in a BMIBMicro vacuum furnace. Carbon- and nitrogen-bearing atmospheres were created by feeding ethylene and ammonia in the stages of carburizing and carbonitriding, respectively (Fig. 1). The pressure, the gas flow, and the duration of such treatments were optimized in order to provide a saturated layer with a thickness of 0.9 mm on the basis of results of the experiments described in detail in [18, 21]. The thickness of the saturated layer was determined from the data obtained by measuring the hardness; the hardness of the layer should exceed 550 HV after quenching.

The concentration profiles of carbon and nitrogen were measured with the help of a LECO analyzer and by the method of glow discharge optical emission spectroscopy, respectively. The metallographic analysis of the carbonitrided layers was performed after etching the metallographic specimens in Nital and Murakami reagents. The hardness profiles were obtained using a Buehler Micromet 2100 device at a load of 1 N. The maps of distribution of the chemical elements in the carbonitrided samples were obtained with the help of scanning electron microscopy and x-ray diffraction analysis. To determine the phase composition the x-ray diffraction spectra were obtained in cobalt K_α radiation with wavelength 0.1789 nm.

RESULTS AND DISCUSSION

Experimental Studies

Figure 2 presents the microstructure of the studied steels after LPCN (with duration exceeding that in Fig. 1) and oil quenching. The structure of steel B is represented first by martensite and then by bainite in the direction from the surface to the core (Fig. 2a). The surface zone of steel 16MnCr5 (with a thickness of 200 μm) contains retained austenite. Martensite and bainite are detectable at a distance $h = 200 – 500$ μm from the surface. The core of the sample contains perlite and ferrite (Fig. 2b).
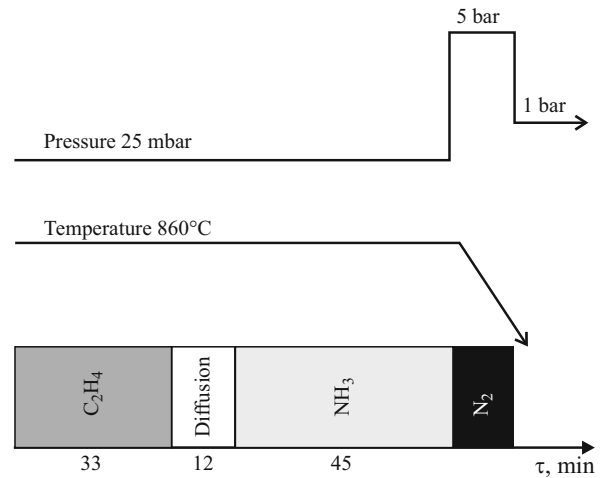
Fig. 1. Scheme of a cycle of low-pressure carbonitriding (LPCN).

The curves of hardness distribution presented in Fig. 3 match the observed structures. In steel B the hardness is approximately constant (800 $HV_{0.1}$) at $h = 0 – 400$ μm and then decreases gradually. In steel 16MnCr5 the hardness decreases in a layer with a thickness of 200 μm, which corresponds to the presence of a "dark component." A maximum hardness (750 – 800 $HV_{0.1}$) is attained at $h = 200 – 400$ μm. Then the hardness decreases upon the appearance of equilibrium components (ferrite and perlite) in the layer at $h = 400 – 700$ μm.

To determine the presence or absence of chromium-bearing carbides we used the Murakami reagent. Such precipitation has not been detected in carbonitrided steel 16MnCr5. This cannot be said about steel B, a typical microstructure of which is presented in Fig. 4. The surface layer of the steel exhibits four zones that correspond to the detected distribution of carbides over the thickness of the sample. From the surface to $h = 90$ μm the fraction of the chromium-bearing carbides is 1.65%. At a distance $h = 90 – 200$ μm the proportion of these carbides attains a maximum (6.4%) and then de-

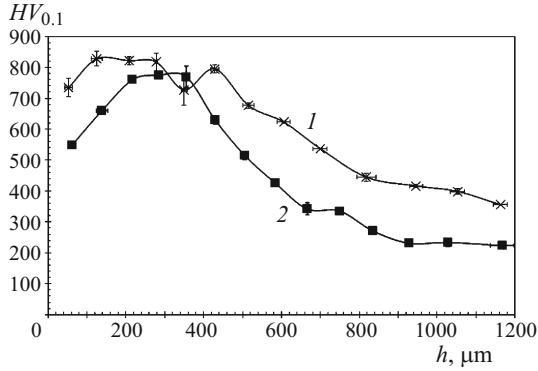**Fig. 2.** Microstructure of steels B (a) and 16MnCr5 (b). Etching with Nital (light microscopy).
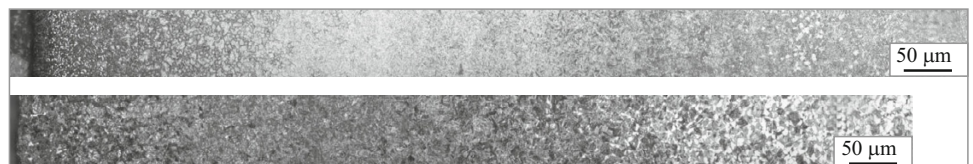
Fig. 3. Distribution of the hardness over the thickness of samples of steels B (1) and 16MnCr5 (2) (h is the distance from the surface).
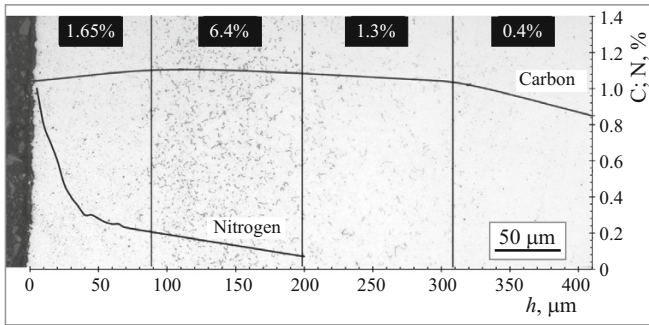

Fig. 4. Carbon and nitrogen profiles imposed on a micrograph of the structure of carbonitrided steel B (h is the distance from the surface). Etching in the Murakami reagent: the data in the dark rectangles present the proportion of the chromium-bearing carbides.

creases gradually to 1.3% ($h = 200 – 310$ μm) and 0.4% ($h = 310 – 400$ μm).

To understand this trend, the profiles of carbon and nitrogen concentrations were imposed on the micrographs obtained after etching steel B in the Murakami reagent (Fig. 4).
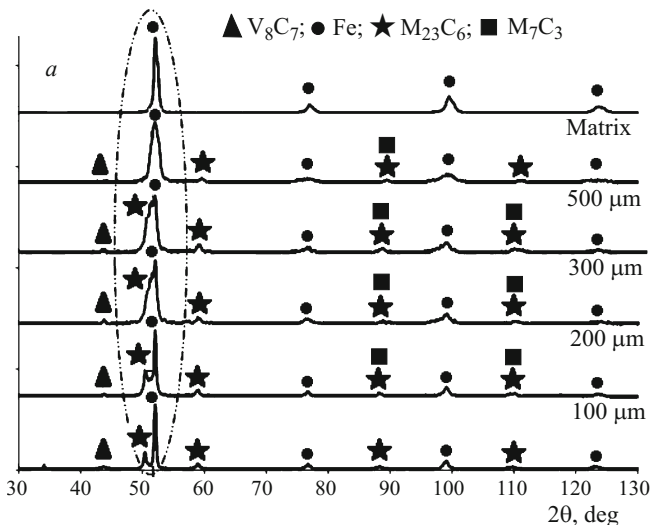
A carbon content exceeding 1 wt.% was observed in a surface layer up to 310 μm thick. A nitrogen content exceeding 0.6 wt.% was preserved in the next layer with a thickness of up to 20 μm and decreased progressively to 0.2 and 0.07% in the layers 100 and 200 μm thick, respectively.

The imposition of the profiles of C and N concentrations on the micrographs reflects the probable effect of nitrogen on the formation of chromium-bearing carbides. Indeed, only the nitrogen concentration varies between the surface and $h = 310$ μm. When the nitrogen content exceeds 0.2%, etching with the Murakami reagent reveals chromium-bearing carbides in an amount of 1.65%. This concentration increases by a factor of 4 (to 6.4%) when the nitrogen content falls below 0.2%.

Finally, when nitrogen is not detected in the surface layer, the fraction of the precipitates containing chromium is the lowest ($< 1\%$).

To obtain diffractograms at different distances from the surface (surface; $h = 100, 200, 300, 500$ μm; core) we removed layers with a specified thickness from carbonitrided samples. It can be seen from Fig. 5 that the diffractograms reflect the presence of $M_{23}C_6$ and V_8C_7 carbides on the surface in addition to the α-phase. At a certain distance from the surface there appear an M_7C_3 carbide. Carbides of types $M_{23}C_6$ and M_7C_3 have also been detected in carbonitrided steels in [22 – 26], where the eutectic $(Fe, Cr)_7C_3$ carbides have exhibited a relative resistance to the heat treatment [23]. On the contrary, the authors of [24, 25] report a transformation of hexagonal M_7C_3 carbides with a very high chromium content into cubic $M_{23}C_6$ carbides upon an appropriate heat treatment. Carbide $M_{23}C_6$ can also be formed due to decomposition of M_7C_3 [24].

Giving data on the types of the carbides ($M_{23}C_6$ and M_7C_3) these studies do not reflect their composition. However, it is obvious that they do contain chromium.

We used the maps of the distribution of elements obtained by scanning electron microscopy (SEM) and energy
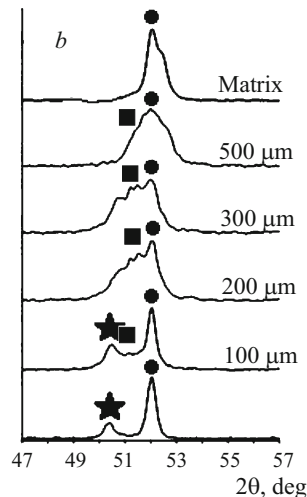

Fig. 5. X-ray diffraction spectra for steel B after low-pressure carbonitriding (vacuum carbonitriding) at different distances from the surface (given at the curves) (a) and an enlarged marked region (b).
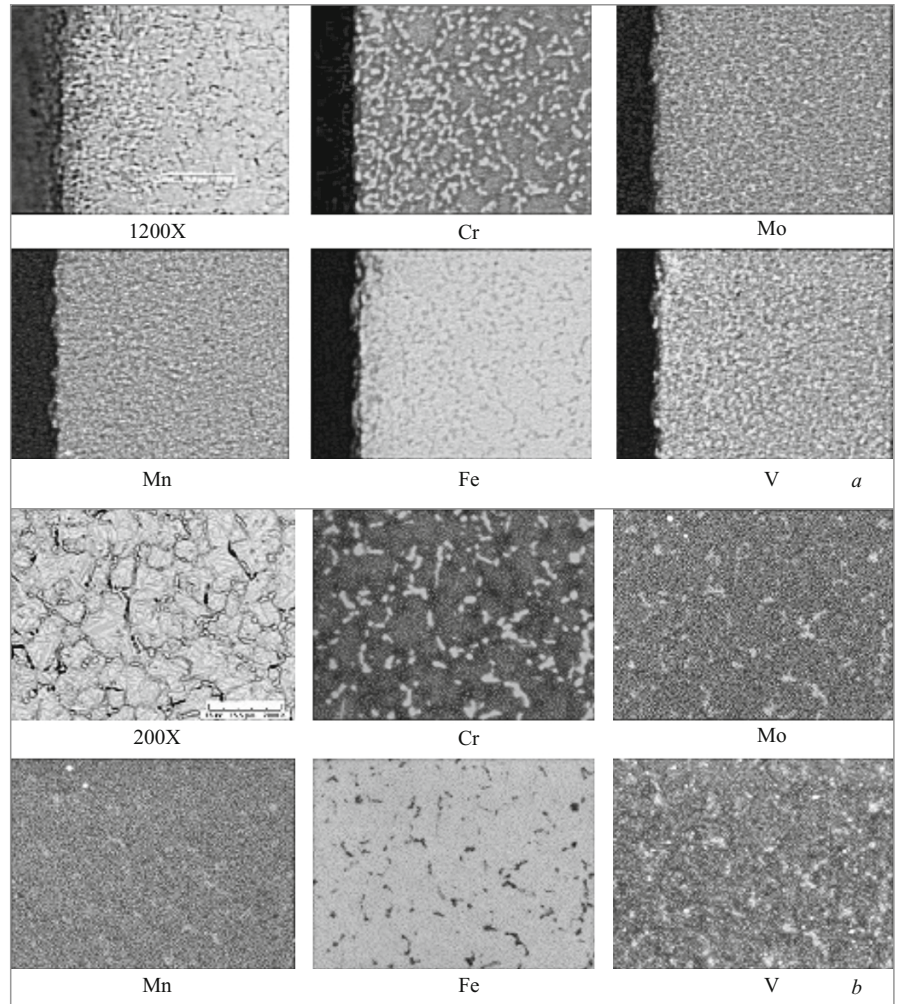
Fig. 6. A map of distribution of elements in carbonitrided steel *B*: *a*) on the surface; *b*) 200 μm from the surface.

dispersive spectroscopy (EDS) to determine the compositions of the precipitates. The measurements were made at different distances from the surface. Figure 6*a* presents a map of elements on the surface, which shows the presence of chromium-rich zones. The chromium-enriched zones coincide with the zones enriched with molybdenum.

Figure 6*b* presents a map of the distribution of elements at a distance $h = 200$ μm. Comparative analysis shows that the regions enriched with chromium and molybdenum are similar to the regions detected on the surface. Moreover, the same zones contain manganese and vanadium.

We suggest two hypotheses explaining the results, namely, (*1*) different types of carbides (V_8C_7, $M_{23}C_6$ and M_7C_3) coexist at this depth and (*2*) the phase composition of the precipitate varies over the thickness.

With allowance for the experimental results we may be positive that carbonitriding of steel *B* causes formation of chromium-bearing carbide precipitates in the surface layer, which are absent in steel 16MnCr5. However, the results of the x-ray diffraction phase analysis should be accepted with caution (the limit of detection of a phase is at least $3 - 5\%$). The map of the distribution of the chemical elements widens

the information on the composition of the surface layers. At least we may be positive that the diffusion layer, according to the data of the x-ray diffraction analysis, contains different carbides (V_8C_7, $M_{23}C_6$ and M_7C_3, Fig. 5).

Thermodynamic Simulation

It impossible to determine exactly the chemical composition of the metallic component M in the $M_{23}C_6$ and M_7C_3 carbides detected with help of x-ray diffraction, which justifies the attention to thermodynamic computational tools. We used the Thermo-calc® classical software (version *R*) to make thermodynamic computations.

Phase Distribution. We started with thermodynamic computations for determining the distribution of the phases over the thickness. The computation was based on the concentration profiles of carbon and nitrogen and gave us only the presence of an austenitic phase. This phase in steel 16MnCr5 is enriched with carbon and nitrogen. No other phase is predictable, which agrees with experimental results.

A similar approach was applied to steel *B*. In contrast to the results obtained for 16MnCr5, we predicted the appearance of many other phases for this grade. Indeed, the curves
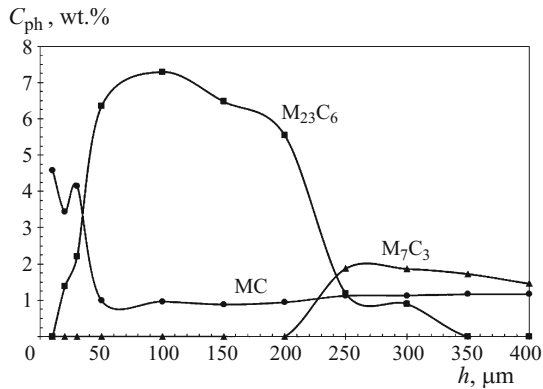
Fig. 7. Computed distribution of phases (C_{ph} is the phase content) over the thickness of carbonitrided layer for steel *B*.

of the phase distribution (Fig. 7) reflect the presence of carbides of types $M_{23}C_6$ and M_7C_3 and an MC carbide with an fcc lattice in addition to the austenite.

The weight fraction of the precipitates varies over the thickness of the layer (and thus depends on the content of carbon and nitrogen). At a distance of about 100 μm from the surface the weight percent of the precipitates is the highest (8.25%).

The surface contains only an MC carbide in an amount of 4.33 wt.%. The content of this carbide decreases to 1 wt.% almost linearly until $h = 50$ and then remains invariable. Starting with $h = 10$ μm the weight fraction of carbide $M_{23}C_6$ increases rapidly and attains 7.3 wt.% at $h = 100$ μm. Then the concentration of this phase decreases and should be zero at $h > 350$ μm according to the computation. The decrease in the content of $M_{23}C_6$ coincides with precipitation of an M_7C_3 carbide, which appears after $h = 200$ μm. The content of this carbide attains 1.87 wt.% and is preserved at this level at $h > 250$ μm.

Phase Composition. The variation of the phase composition over the thickness of the specimens was estimated simultaneously with computing the distribution of the concentration profiles of the alloying elements. The content of the fcc austenite phase exceeds 91.7 wt.%. It also contains the whole of the nickel over the whole of the thickness of the diffusion layer. The same concerns the manganese until the appearance of an M_7C_3 carbide that contains a little more than a half of the manganese of the matrix. The MC phase with an fcc lattice contains the whole of the vanadium of the steel. Being the only precipitate at $h = 10$ μm it also contains the entire chromium, molybdenum, tungsten and nitrogen. At this depth the stoichiometry of the MC phase corresponds to a carbonitride with composition $Cr_{0.68}V_{0.22}Mo_{0.05}W_{0.03}Fe_{0.02}(C_{0.15}N_{0.85})$.

At $h > 20$ μm the precipitated $M_{23}C_6$ carbide takes the whole of the chromium, molybdenum, tungsten and, especially, carbon from the MC carbonitride with fcc lattice. The composition of the MC phase shifts gradually to a vanadium nitride and becomes $V_{0.91}Fe_{0.05}Cr_{0.037}W_{0.002}Mo_{0.001}(C_{0.03}N_{0.97})$

at $h = 50$ μm. It should be noted that whatever the thickness of the diffusion layer, nitrogen is contained in the MC phase exclusively. At $h = 100$ μm the $M_{23}C_6$ carbide takes virtually the whole of tungsten, molybdenum, chromium and carbon and is describable by the formula $(Fe_{0.75}Cr_{0.21}Mo_{0.027}W_{0.013})_{23}C_6$. At $h > 200$ μm the precipitated M_7C_3 carbide takes carbon and chromium from the $M_{23}C_6$ carbide, the proportion of which decreases progressively over the thickness of the layer. Thus, the elements contained initially in the $M_{23}C_6$ carbide are redistributed and go into carbides of types MC and M_7C.

We assume that the presence of nitrogen hinders the precipitation of the M_7CC_3 carbide appearing at $h = 250$ μm, after which the concentration of nitrogen is reduced to zero. Starting with $h = 350$ μm the layer does not contain precipitates of type $M_{23}C_6$. The M_7C_3 carbide becomes a prevalent chromium carbide and has composition $(Cr_{0.499}Fe_{0.452}V_{0.037}Mn_{0.007}W_{0.005})_7C_3$.

CONCLUSIONS

1. After low-pressure carbonitriding of low-alloy steels with 0.16 – 0.18% C the concentration of the alloying elements (Cr, Mn, V, W, Mo) in their diffusion layer increases, which causes the appearance of chromium-bearing carbides of types MC, $M_{23}C_6$ and M_7C_3.

2. The prevalent carbide in the diffusion layer of the carbonitrided steels is MC, which is replaced gradually by an $M_{23}C_6$ carbide, while an M_7C_3 carbide appears in the deeper layers free of nitrogen.

3. The data of the layer-after-layer phase analysis and the maps of the distribution of the elements agree well with the thermodynamic computations of the phase composition of the diffusion layer in the steels studied after low-pressure carbonitriding.

REFERENCES

1. G. F. Bocchini, "Overview of surface treatment methods for PM parts," *Adv. Powder Metall. & Partic. Mater.*, **6**, 56 – 87 (2001).
2. *Metals Handbook, Heat Treating*, ASM Int. (1991), Vol. 4.
3. H. Ferguson, "Heat treatment of ferrous powder metallurgy parts," in: *Powder Metal Technologies and Applications, A Handbook*, ASM Int., Metals Park (1998), Vol. 7, pp. 645 – 655.
4. P. F. Stratton and L. Sproge, "Gaseous carburizing and carbonitriding: the basics," *Heat Treat. Met.*, **31**(3), 65 – 68 (2004).
5. A. Goldsteinas, "New vacuum processes achieve mechanical property improvement in gearbox components," *Gear Technol.*, **24**(6), 34 – 39 (2007).
6. W. Grafen, O. Irretier, and M. Rink, "Applications of low-pressure carburization with high temperatures (1000°C to 1050°C) in industrial practice," *Heat Treat. Met.*, **62**(3), 97 – 102 (2007).

7. S. Kremel, H. Danninger, H. Altena, and Y. Yu, "Low-pressure carburizing of sintered alloy steels with varying porosity," *Powder Metall. Progr.*, **4**(3), 119 – 131 (2004).

8. D. Ghiglione, C. Leroux, and C. Tournier, "Nitruration, nitru-carburation et derives," in: *Pratique des Traitements Thermochimiques*, Editions Techniques de l'Ingénieur, Association Technique de Traitement Thermique (ATTT), [M 1 227] (1996).

9. D. H. Herring and J. C. St. Pierre, "Vacuum carburizing of P/M steels," *Annual Powder Metallurgy Conference Proc.*, **43**, 525 – 537 (1987).

10. H. Altena and F. Schrank, "Low-pressure carbonitriding using acetylene and ammonia – a novel diffusion process for case-hardening," *Heat Treat. Met.*, **58**(4), 204 – 210 (2003).

11. P. Jacquet, D. R. Rousse, G. Berdard, and M. Lambertin, "A novel technique to monitor carburizing processes," *Mater. Chem. Phys.*, **77**, 542 – 551 (2002).

12. K. Kawata and S. Asai, "Atmosphere control during low-pressure carbonitriding processes," in: *17th Int. Fed. for Heat Treat. and Surface Eng. Congr.* (2008), pp. 327 – 330.

13. J. Slycke, "Carbonitriding – an investigation from the process point of view," *Thèse, Linköping Studies in Science and Technology, Dissertation No. 37* (1979).

14. E. Gianotti, "Algorithm for carbon diffusion computation in a vacuum furnace," *Heat Treat. Progr.*, **2**, 27 – 30 (2002).

15. J. Goldstein and A. Moren, "Diffusion modeling of the carburization process," *Metall. Mater. Trans. A*, **9**(11), 1515 – 1525 (1978).

16. R. Gorockiewicz, "The kinetics of low-pressure carburizing of alloy steels," *Vacuum*, **86**(4), 448 – 451 (2011).

17. M. Jung, S. Oh, and Y. Lee, "Predictive model for the carbon concentration profile of vacuum carburized steels with acetylene," *Metals Mater. Int.*, **15**(6), 971 – 975 (2009).

18. T. Marray, "Carbonitruration basse pression d'aciers et de pièces obtenues par la Technologie MIM," in: *Thèse Arts et Mètiers ParisTech, ENAM-0056* (2012), 143 p.

19. H. Berns and A. Fischer, "Microstructure of Fe – Cr – C hardfacing alloys with additions of Nb, Ti and B," *Mater. Charact.*, **39**, 499 – 527 (1997).

20. L. Lu, H. Soda, and A. McLean, "Structural materials: properties, microstructure and processing," *Mater. Sci. Eng. A*, **347**, 214 – 222 (2003).

21. T. Marray, P. Jacquet, D. Checot, and F. Fabre, "Carbonitriding treatment applied to PIM elaborated parts," in: *Proc. World PM2010 Conf., 10 – 14 October 2010, Florence, Italy* (2010), Vol. 2, pp. 489 – 494.

22. S. D. Carpenter and D. Carpenter, "X-ray diffraction study of M_7C_3 carbide within high chromium white iron," *Mater. Lett.*, **57**, 4456 – 4459 (2003).

23. G. N. Laird and G. L. F. Powell, "Solidification and solid state transformation mechanisms in Si alloyed high-chromium white cast irons," *Metall. Trans. A*, **24**, 981 – 988 (1993).

24. X. Wu and G. Chen, "Microstructural features of an iron-based laser coating," *J. Mater. Sci.*, **34**, 3355 – 3361 (1999).

25. J. T. H. Pearce and D. W. L. Elwell, "Duplex nature of eutectic carbides in heat-treated 30% chromium cast iron," *J. Mater. Sci. Lett.*, **5**, 1063 – 1064 (1986).

26. S. Buytoz, "Microstructural properties of M_7C_3 eutectic carbides in a Fe – Cr – C alloy," *Mater. Lett.*, **60**, 605 – 608 (2006).